Published in final edited form as:

Traffic. 2017 July ; 18(7): 453–464. doi:10.1111/tra.12486.

Abnormal Rab11-Rab8-vesicles cluster in enterocytes of patients with Microvillus Inclusion Disease

Georg F. Vogel[1,2,3], **Andreas R. Janecke**[3], **Iris M. Krainer**[2,3], **Karin Gutleben**[1], **Barbara Witting**[1], **Sally G. Mitton**[4], **Sahar Mansour**[5], **Antje Ballauff**[6], **Joseph T. Roland**[7], **Amy C. Engevik**[7], **Ernest Cutz**[8], **Thomas Müller**[3], **James R. Goldenring**[7], **Lukas A. Huber**[2,*], and **Michael W. Hess**[1,*]

[1]Division of Histology and Embryology, Medical University of Innsbruck, Austria

[2]Division of Cell Biology, Medical University of Innsbruck, Austria

[3]Department of Paediatrics I, Medical University of Innsbruck, Austria

[4]St. George's University Hospitals, London, UK

[5]Human Genetics Research Center, St. George's University of London, UK

[6]Helios Klinikum Krefeld, Germany

[7]Section of Surgical Sciences, Epithelial Biology Center, and Department of Cell & Developmental Biology, Vanderbilt University School of Medicine, Nashville, TN, USA

[8]Division of Pathology, Department of Paediatric Laboratory Medicine, The Hospital for Sick Children, Toronto, Ontario, Canada

Abstract

Microvillus Inclusion Disease (MVID) is a congenital enteropathy characterized by accumulation of vesiculo-tubular endomembranes in the subapical cytoplasm of enterocytes, historically termed "secretory granules". However, neither their identity nor pathophysiological significance is well defined. Using immunoelectron microscopy and tomography we studied biopsies from MVID patients (3x Myosin 5b mutations, 1x Syntaxin3 mutation) and compared them to controls and genome-edited CaCo2 cell models, harboring relevant mutations. Duodenal biopsies from two patients with novel Myosin 5b mutations and typical clinical symptoms showed unusual ultrastructural phenotypes: aberrant subapical vesicles and tubules were prominent in the enterocytes, though other histological hallmarks of MVID were almost absent (ectopic intra-/intercellular microvilli, brush border atrophy). We identified these enigmatic vesiculo-tubular

*Correpondence to: Michael.Hess@i-med.ac.at or Lukas.A.Huber@i-med.ac.at.

List of Supplementary Materials

Figure S1 is related to text figure 1 and table 1. It complements the illustration of the small intestine phenotype of the here described new MVID cases (i.e., patients #1 and #2).

Figure S2 is related to text figs. 3 & 4 and provides additional, complementary double-label IEM data.

Figure S3 is related to text figures 3 & 4 and illustrates IEM labeling patters obtained from the genome-edited CaCo2 cell models of MVID, for complementing the respective data from patient biopsies.

Table S1 lists the primers used for sequence analysis of the here newly described MVID patients #1 and #2.

Movie S1 is related to text figure 1B, C showing tomographic reconstruction and 3D-modelling of the here characterized abnormal Rab11-Rab8-endomembranes in MVID.

organelles as Rab11-Rab8-positive recycling compartments of altered size, shape and location harboring the apical SNARE Syntaxin3, apical transporters Sodium-Hydrogen Exchanger 3 (NHE3) and cystic fibrosis transmembrane conductance regulator (CFTR). Our data strongly indicate that in MVID disrupted trafficking between cargo vesicles and the apical plasma membrane is the primary cause of a defect of epithelial polarity and subsequent facultative loss of brush border integrity, leading to malabsorption. Furthermore, they support the notion that mislocalization of transporters, such as NHE3 substantially contributes to the reported sodium loss diarrhea.

Keywords

immunoelectron microscopy; electron tomography; Rab Small GTPases; Rab11a; Rab8a; Stx3; Myo5b; NHE3; hereditary enteropathy; congenital diarrheal disorder

1. INTRODUCTION

Microvillus inclusion disease (MVID; OMIM 251850) is a rare, usually fatal hereditary enteropathy characterized by quite remarkable, complex ultrastructural alterations (see (1, 2), for the original descriptions and (3), for a review). Clinically, MVID presents with intractable watery diarrhea, partial sodium loss and nutrient malabsorption during the first days or months after birth (1, 4). Classical histological hallmarks are villus atrophy in the small intestine and partial absence of the epithelial brush border, together with aberrant intracellular accumulation of periodic acid-Schiff (PAS)-positive material (1, 2).

In the majority of genetically verified cases known so far (n=~70, our unpublished data) MVID results from mutations in the motor protein Myosin 5b (Myo5b; see (4), for a review), as first described by our group (5). Furthermore, we detected the mutated soluble N-ethylmaleimide-sensitive factor attachment protein receptor (SNARE) protein Syntaxin3 (Stx3) to cause a less severe form of enteropathy, considered as a variant form of MVID (6). Mutations in both *MYO5B* and *STX3* disrupt trafficking between apical cargo vesicles and the plasma membrane (7). However, neither MVID pathophysiology nor the subcellular phenotype of the affected absorptive cells (enterocytes) has been fully defined.

In particular, initial electron microscopy (EM) revealed several structural abnormalities specific for MVID (1). Firstly, the densely packed apical microvilli, normally forming the enterocytes' brush border, are partially or totally disrupted. Secondly, microvilli of villus enterocytes do occur ectopically. They are either lining ~2 μm wide, spherical intracellular lumina (termed microvillus inclusions: (2)), or occur at the basolateral plasma membrane in brush-like assemblies. Thirdly, large number of spherical to elongated, ~200 nm-wide, vesicular compartments are observed in the subapical cytoplasm of both crypt and villus enterocytes. Because of their morphology they were tentatively interpreted as (aggregates of) "secretory granules" (1, 3) – bona fide exocytic compartments (8) that are normally confined to undifferentiated crypt cells (e.g., Ref. (9): Fig. 3, Ref. (10): Fig. 3, Ref. (11): Fig. 14), and differ from granules of Paneth cells, enteroendocrine cells or goblet cells. Cytochemical studies showed these conspicuous compartments in the enterocytes of MVID patients further as PAS-positive endomembrane networks (12), that were locally positive for brush border

constituents (13, 14). Nevertheless, the exact nature of these seemingly pleiomorphic organelles has not been defined, nor their possible relevance for the pathophysiology of MVID.

Here we thoroughly analyzed these compartments in tissue samples from patients, including two new cases with an unorthodox MVID phenotype, and in genome-edited human cell models by using complementary microscopy techniques. Our approach allowed us to identify these so far ill-defined structures as Rab11- and/or Rab8-positive recycling endomembrane compartments, enriched with relevant apical membrane proteins, such as Stx3 as well as sodium-hydrogen exchanger 3 (NHE3) and cystic fibrosis transmembrane conductance regulator (CFTR). The data strongly suggest disrupted trafficking between cargo vesicles and the apical plasma membrane as the primary defect in MVID. This presumably leads to loss of epithelial polarity and facultative brush border atrophy, accounting for the sodium loss diarrhea.

2. RESULTS

We studied duodenal, jejunal and colon biopsies from three patients with novel or with published *MYO5B* mutations and in one patient with a *STX3* mutation, as well as genome edited CaCo2 cell models (6, 15), plus controls (i.e., patients with non-MVID related intestinal diseases; wildtype CaCo2 cells). Transmission electron microscopy (TEM) was combined with electron tomography, PAS-cytochemistry (16), immuno-EM, and –in case of limited material–immunofluorescence microscopy (IF). Furthermore, DNA sequence analysis was performed on blood samples from patient 1 and 2.

2.1. Clinical findings & Genetics

Patient 1 (male; *MYO5B*) had intermittent episodes of intractable diarrhea and poor growth from the first few months of life. MVID was diagnosed in his 5-year old sister during her first year of life, and the ultrastructural analyses of their diagnostic intestinal biopsies were suggestive of MVID. These affected siblings were born to consanguineous Asian parents. The affected sister could be weaned from total parenteral nutrition during her 4th year of life. Sanger sequencing of the complete coding region (40 exons) and all flanking exon-intron boundaries of the *MYO5B* gene encoding Myosin 5b was performed in the index patient, i.e., the older affected sibling of patient 1, revealing a homozygous *MYO5B* mutation c. 244G>A (p.Glu82Lys) in exon 3. Targeted sequencing of exon 3 in family members revealed the same mutation in homozygous state in patient 1 and in heterozygous state in both healthy parents. Results are based on NCBI mRNA reference sequence NM_001080467, in which the A of the ATG translation initiation codon was nucleotide 1. Primers are listed in Supplementary Table S1. The c.244G>A (p.Glu82Lys) mutation is very rare; it is not listed in public databases including the Exome aggregation consortium database, EXAC. The p.Glu82Lys mutation affects a highly conserved amino acid, and is a non-conservative amino acid substitution, which is likely to impact secondary protein structure, as these residues differ in polarity, charge, and size, all of which is supported by *in-silico* analyses (SIFT, PolyPhen2). The identified *MYO5B* missense mutation might still preserve residual Myo5b protein function.

Patient 2 (male; *MYO5B*) is the second child of healthy Asian patients who were not aware of any consanguinity between them, and he has a healthy sister. He started to have an intractable secretory diarrhea from birth, requiring total parenteral nutrition. An analysis of the whole coding region and all splice-sites of *MYO5B* revealed homozygosity for a c. 414C>A (p.His138Gln) mutation in exon 4. The c.414C>A (p.His138Gln) mutation is very rare; it is not listed in public databases including the Exome aggregation consortium database, EXAC. The p.His138Gln mutation affects a highly conserved amino acid, and is a non-conservative amino acid substitution, which is likely to impact secondary protein structure, as these residues differ in polarity and size, all of which is supported by *in silico* analyses (SIFT, PolyPhen2).

Patient 3: *MYO5B* c.1323–2A>G was described previously (4, 17).

Patient 4: *STX3* c.372_373dup (p.Arg125Leufs*7) was described previously (6).

2.2. TEM-morphology and PAS-cytochemistry

In the biopsies from all four MVID patients distinct accumulations of ~100 to 400nm-wide, pleomorphic endomembrane compartments occupied the subapical cytoplasm of a high percentage of enterocytes (Fig. 1A). Three-dimensional (3D) reconstruction using electron tomography confirmed mainly isolated vesicles, as well as partly branching, interconnected tubular compartments (Fig. 1B, C; Movie S1). These endomembrane aggregates reached frequently from the perinuclear area to the plasma membrane, or the terminal web, where still present. Neighboring, unaffected enterocytes and controls showed scattered vesicles and short tubules, likely early and recycling endosomes and/or exocytic vesicles. Similar patterns were seen in genome-edited and control CaCo2 cell models (see Fig. S1D in Ref. (15)).

In conventionally stained plastic- and cryo-sections the contents of the vesicles/tubules appeared homogeneously electron-dense or -lucent (Fig. 1A, B). Locally, dense compartments were continuous with lucent ones, including parts with mixed contents (Fig. 1A). Dense vesicles/tubules were found preferentially, though not exclusively, in the crypts (Fig. 1B). Lucent ones occurred all along the villi, where they frequently surrounded also microvillus inclusions, but also sporadically in the crypts. The relative abundance of dense and lucent vesicles/tubules varied throughout the samples and between the patients. Genome-edited CaCo2 cell models showed predominantly lucent vesicles/tubules (see Fig. 1G in Ref. (15)).

Consistent with previous studies (12), most of these vesicles/tubules proved PAS-positive (Fig. 1C, D, E); and so did late endosomes/multivesicular bodies, the huge, quite heterogeneous population of degradative compartments (lysosomes, autophagosomes; (Fig. 1D, Figure S1D)), the glycocalyx and substances contained within the lumina of microvillus inclusions (Figure S1B). PAS-staining intensity of the vesicles/tubules was not uniform, but PAS-reactive material was also detectable within the lucent vesicles/tubules thanks to special preparation and incubation protocols (Fig. 1E, F; for further details see the Materials and methods paragraph). In control biopsies, we merely observed a few dense, ~200 nm wide, PAS-positive vesicles (and occasionally short tubules) in the apical cytoplasm of immature crypt enterocytes (Fig. 1G).

Taken together, the vast majority of the subapically clustering vesicles and tubules in the here presented MVID patients and genome-edited human CaCo2 cell lines were identical to structures historically termed “secretory granules”, as originally described from enterocytes of MVID patients (1, 2).

The other ultrastructural hallmarks of MVID are shortened and/or lacking brush border microvilli, as well as microvillus inclusions and/or basolateral microvilli. Notably, these features were rare or possibly even absent in the newly described patients 1 and 2 with mutated *MYO5B* (based on data available so far; Figure S1A–C), but prominent in *MYO5B* patient 3 (see Fig. 4A in ref. (17)). Patient 4 with a *STX3* mutation showed few microvillus inclusions, but consistently basolateral microvilli (see Fig. 1D in Ref. (6). Denuded enterocytes occurred regularly in this patient, not only along the villi, but prominently also in the crypts (Figure S1D); such features have so far not been reported in any case of MVID, but could be also observed in two other, yet undescribed cases with *STX3* mutations (our unpublished observations). Table 1 summarizes the varying subcellular phenotypes in enterocytes from the MVID patients and in the cell models presented here. In addition, drawings (Figure 2) illustrate in a generalized manner the predominant ultrastructural features of MVID enterocytes as compared to healthy controls.

2.3. Immunolabeling

To characterize the enigmatic vesicles/tubules and attribute them to a well-defined class of organelles we performed immunogold labeling on thawed cryo-sections (complemented with IF and pre-embedding IEM for patient 2). Biopsies and CaCo2 lines were probed with antibodies against membrane proteins that control proper trafficking of apical cargo in polarized epithelia, but show unorthodox, subapical IF-signals in MVID tissues and models. Amongst them, the small GTPase Rab11 appeared as a highly promising candidate (17–19). Indeed, in MVID samples and all genome-edited cell models presented here Rab11 was consistently seen at the membranes of subapically accumulating vesicles/tubules (Fig. 3A–C). To a minor extent Rab11 could also be detected in the cytoplasm, at the Trans Golgi network (TGN), brush border remnants and lateral plasma membrane domains (Tab. 2). Three different anti-Rab11/Rab11a antibodies gave almost identical results. Similarly, another key player in targeted transport of exocytic vesicles, Rab8a, also occurred regularly at the membranes of the subapical vesicles/tubules (Fig. 3D, E), in addition to its canonical distribution (Tab. 2). In the controls these markers were confined to their typical locations as reported from IEM (20–23) and IF-studies.

As a member of the Rab11-Rab8 cascade the t-SNARE Stx3 mediates fusion of exocytic vesicles with the apical plasma membrane (7, 24–26). In samples lacking functional Myo5b, Stx3 was consistently found associated with subapical vesicles/tubules (Fig. 4A, B) and throughout the subapical cytoplasm, together with only moderate labeling of the apical plasma membrane (Fig. 4B). In the controls, Stx3 was located predominantly at the brush border, whereas the *STX3*-mutant biopsy and the respective genome-edited CaCo2 cell models showed no labeling at all (Tab. 2).

Furthermore, of particular interest was the distribution of apical transporters, since mislocalization of NHE3 and CFTR had been reported from intestinal epithelia of MVID-

patients (19, 27). In biopsies of duodenum from our MVID patients, anti-NHE3 strongly labeled lucent and dense vesicles/tubules (Fig. 4C, D), the endoplasmic reticulum, and to a minor extent, the brush border (Tab. 2). Similar results were obtained with HA StrepTactin II (HS) tagged NHE3 and CFTR expressed in the genome-edited CaCo2 models (e.g., Figure S3A, B). Controls showed normal distribution of NHE3 (and HS-CFTR). Double labeling experiments complemented these observations (Fig. 3E, Figure S2A, B), though the respective labeling densities were considerably lower than with one marker only. Occasionally, immunogold label of cargo (endogenous or tagged), Stx3 or Rab8a on the one hand, and Rab11a on the other hand, was apparently located at the very same, distinct structural entity (i.e., one and the same vesicle/tubule; e.g., Figure S2A).

Markers for late endosomes and (autophago)lysosomes specifically labeled their respective compartments (e.g., Lamp1 (Lysosomal acid membrane protein1): Fig. 4E; LBPA (Lysobisphosphatidic acid), or p62/SQSTM1 (sequestosome-1): data not shown). Subapical vesicles/tubules, however, remained generally unstained (Fig. 4E), except for very few cases where dense tubules were evidently connected with Lamp1-positive organelles.

In addition, we performed immunofluorescence microscopy for Rab11, Stx3 and NHE3 (Figure 5) as well as pre-embedding IEM for Rab11 (not shown) with biopsies from patient 2 because of limited material. The data generally supported our IEM findings and were consistent with the literature.

Finally, biopsy specimens from patient 4 with mutated *STX3* provided the unique opportunity to document the IEM localization of endogenous Myo5b in the vicinity of vesicular compartments. Whereas control biopsies showed a rather inconspicuous distribution of Myo5b throughout the (sub)apical cytoplasm and at the apical plasma membrane, Myo5b was regularly found at membranes of the vesicles and tubules in enterocytes of patient 4 (Fig. 6A, B). Enterocytes from MVID patients with *MYO5B* mutations were devoid of label, except for some negligible background that could result from aberrant expression of Myo5b mutants (Figure 6C). Similar data were obtained from a Myo5b-rescue cell line (Myo5b KI HS-Myo5b: (15)). HS-Myo5b was found close to (Rab11-positive) vesicular/tubular compartments in the cell periphery (Figure S3C, D), at the apical plasma membrane in the vicinity of Stx3, and throughout the (sub)apical cytoplasm.

3. DISCUSSION

Ever since the original descriptions of MVID (1, 2) subapical aggregates of vesicles and tubules, tentatively interpreted as “secretory granules”, were consistently recognized as specific, pathological feature of crypt, but also villus enterocytes of most MVID patients investigated (28). EM-cytochemistry according to Thiéry (16) -the ultrastructural correlate to PAS-staining- showed these structures, as well as the abundant (autophago)lysosomes to account together for the broad band of intracellular PAS-staining seen with light microscopy ((12) and the present study). However, further information on the identity and biochemical properties of these compartments has been scarce so far, except for two case reports, where

sporadically sucrase isomaltase (SI: (13)) or Lewis histo-blood group antigen Le-a (14) was detected by IEM.

In the present study we used complementary microscopy techniques for characterizing the MVID-specific vesicles/tubules in enterocytes from intestinal biopsies of patients and in the genome-edited CaCo2 cell models (altogether: x4 *MYO5B*, x2 *STX3* mutations; see Tab. 1). Our comparative IEM analyses yielded highly congruent results (Tab. 2), irrespective of patient-specific variations of ultrastructural and clinical phenotypes and regardless of the *MYO5B* or *STX3* mutations involved.

All members of the Rab11-Rab8 cascade, as well as the cargo molecules studied here were regularly located in association with the membranes of dense and lucent vesicles/tubules and throughout the subapical cytoplasm, in addition to their canonical distribution. These were Rab11/Rab11a, Rab8a and Stx3 or Myo5b, plus the transporters NHE3 and CFTR. Of them, Rab11a and Rab8a may serve as bona fide organelle markers for recycling system membranes (e.g., (20, 29–31)), though strict organelle classifications might fall short in the light of the highly disordered subcellular context of MVID. Most remarkable is the distinct, robust signal of Rab11/Rab11a (32–34) in the subapical cytoplasm of human and mouse tissues and cell models ((17–19, 35); and the present study). Given our previous observation (36) of ultrastructural similarities to branched recycling tubules (37), one could interpret this subapical vesiculo-tubular network as abnormally extended, aberrant apical recycling endosomes.

The data on NHE3 and CFTR distribution presented here in MVID biopsies and/or models support this explanation, since intracellular trafficking of these transporters involves recycling compartments (38–42). It would also be conceivable to emphasize the role of Rab11a in secretory trafficking (32, 43, 44). The expanded vesiculo-tubular Rab11a-containing endomembrane system may reflect blockade of processing of constitutive and regulated secretory pathways through the apical recycling system. Both points of view are not mutually exclusive and furthermore compatible with the observed Rab8a distribution. As shown here by IEM, the partial mislocalization of Rab8a clearly included the subapical vesicles/tubules, though previously reported IF-patterns (18, 19, 35) appeared less defined as compared to Rab11a. Among others, Rab8a regulates biosynthetic traffic ((45–47), for review), and localizes, therefore, both to secretory vesicles and recycling compartments (20, 48–54). In sum, we provided here a provisional diagnosis of MVID-specific sub-apical vesicules/tubules as abnormal Rab11-Rab8-positive endomembranes, harboring also mislocalized apical proteins, some of which are subject to recycling.

Our observation that proteins involved in apical vesicle traffic were differentially distributed throughout the endomembrane network in MVID enterocytes needs further detailed investigation. With the available antibodies it was possible to perform double labeling for Rab11a in comparison to Rab8a, Stx3 or NHE3 (but not for Rab8a together with Stx3 or NHE3). Unambiguous co-localization on the very same vesicle/tubule was rarely detectable, despite the robust labeling for these proteins across the entire subapical area. The failure to detect simultaneously Rab11a and Rab8a on one and the same vesicle/tubule is not surprising. The gross distribution of these Rab GTPases generally shows variable degrees of

overlap (55): from very low in many cell types (e.g. (56)), to quite high (e.g., (57, 58)). Moreover, according to current concepts of apical cargo exocytosis/recycling, Rab11a recruits Rab8a to the vesicles via guanine exchange factor interaction for proper transport to the apical domain (7, 59, 60). Thus, both Rab proteins are required for Myo5b to interact with the apical Stx3 (15). As Stx3 interacts with the GTPase activating factors for both Rab11a and Rab8a (15), the transient binding of the Rab proteins to the vesicles is soon terminated at the apical plasma membrane. The presumably narrow time-frame of co-localization during the highly dynamic apical exocytosis/recycling (31, 61) likely reduces the probability of detecting such features by static IEM; not to forget also the limitations inherent to IEM-analyses of complex, extended 3D structures by using ultra-thin sections.

The seemingly not congruent distribution of Rab11a and apparently trapped cargo or Stx3 points to the possible existence of sub-domains within the recycling system network, as, for example, defined previously by members of the family of Rab11-interacting proteins (Rab11-FIPs) (62, 63). Intriguingly, the sub-compartmentation of the MVID-specific subapical endomembranes postulated here does not seem to correlate directly with the allocation of the (still undefined) dense and +/− lucent matrix contents within these vesicles/tubules. Thus, this hypothetical sub-compartmentation requires further analyses, as well as the previously reported phenomenon of cargo-selectivity in apical trafficking (15). In certain cases of mutated *MYO5B*, only selected apically destined cargoes apparently mislocalize subapically, while other cargoes do not (e.g. NHE3, CFTR, GLUT5 versus DPPIV, SI, APN: (15), and our unpublished results; see also (64) in this context). Conceivably, several apical trafficking routes, presumably diverging at the TGN or further upstream at the apical recycling endosomal compartment with its potential sub-compartmentation, should be taken into account.

Together, our major findings are as follows: Two MVID patients with novel *MYO5B* mutations presented with typical clinical symptoms and abundant subapical vesicles and tubules, but quite intact brush border and almost no ectopic microvilli. By using high-resolution microscopy we identified the PAS-positive subapical compartments (historically: “secretory granules”) as Rab11a- and Rab8a-positive, vesiculo-tubular endomembranes of altered extension and position, possibly comprising different sub-compartments. Moreover, the vesiculo-tubular membranes regularly accommodated Stx3, a key element of vesicle exocytosis, as well as apical transporters (NHE3, CFTR). Loss of intestinal NHE3 function causes severe diarrhea in humans (65–67) and mice, suggesting again that NHE3 mislocalization (15, 68) significantly contributes to the reported secretory diarrhea. Thus, we provide further substantial, IEM-based evidence for the concept of disrupted apical traffic (2, 3, 15, 27) and mistargeting of pivotal apical transporters as the primary cause of diarrhea and malabsorption in MVID.

4. MATERIALS AND METHODS

4.1. Human biopsy samples and Genetics

Written informed consent from the patients’ parents was obtained and snap biopsies from duodenal, jejunal, and colonic sites were obtained. Written informed consent for testing of MVID genes or genome-wide testing was obtained from the patients’ parents following

genetic counseling. The study was approved by the Ethics committee of the Medical University of Innsbruck (study no. UN3987) according to the principles outlined by the Helsinki declaration.

Genomic DNA from leucocytes was extracted using the MagAttract DNA Mini *M48* Kit (Qiagen, Hilden, Germany). PCR and sequencing was performed as reported (5).

4.2. Antibodies

The following primary antibodies were used: rabbit anti-Rab8a (56), rabbit anti-Rab11 (71-5300, Zymed), rabbit anti-Rab11a (VU57: (69)), mouse anti-Rab11a (8H10: (70)), rabbit anti-Syntaxin3 (ab133750, Abcam), rabbit anti-NHE3/SLC9A3 (HPA036669, Sigma), mouse anti-LAMP1 (H4A3, Developmental Studies Hybridoma Bank), mouse anti-LBPA (courtesy by Jean Gruenberg), guinea pig anti-p62 (PROGEN), chicken anti-Myosin 5b (71), mouse anti-HA.11 (clone 16B12, Covance MMS-101R-500).

4.3. Immunofluorescence microscopy (IF)

Sample preparation of natively frozen tissue and microscopy have been described previously (15, 17).

4.4. Immunogold-EM of thawed cryo-sections (IEM)

We generally processed biopsy and CaCo2-cell culture samples as previously described (72), taking advantage of the improved ultrastructure preservation achieved with a slight modification of the method published by Pujol and colleagues (73). In particular, tissues/cells were pre-fixed with 4% (w/v) formaldehyde dissolved in 0.1M phosphate buffer (pH 7.2; 24 hrs up to several days (including sample shipment); RT), followed by post-fixation with 4% (w/v) formaldehyde in 0.1M sodium borate buffer (pH 11, 1hr; RT). Subsequent sample processing and indirect single and double labelling was performed according to standard protocols (74, 75). Bound primary antibodies were visualized by relevant secondary antibodies (IgG molecules) conjugated to colloidal gold (Fig. 6) and/or by secondary antibodies (Fab' fragments) conjugated to Nanogold (Nanoprobes; Figs. 3, 4 S2, S3). For double labelling we applied primary antibodies simultaneously, followed by detection with Nanogold-conjugates and 10nm-colloidal gold conjugates (in that order; Figs. S2, S3D). Nanogold conjugates, and optionally colloidal gold conjugates were subjected to silver enhancement (HQ-Silver, Nanoprobes).

4.5. Pre-embedding IEM

Frozen tissue (patient #2) was freeze-substituted and rehydrated (76) followed by permeabilization with Triton X (0.05%, 30min at RT), indirect immunogold labelling (using Nanogold-conjugates), silver enhancement, en-bloc staining with OsO4 and UA and, finally, epoxy resin embedding (77).

4.6. PAS cytochemistry at EM-level

Standard incubations were performed according to Thiéry (16) as described (36). In case of weak staining (e.g., Fig. 1E) incubation with periodic acid (PA) and thiocarbohydrazide (TCH) was optionally extended up to 15hrs each (16), and/or silver proteinate treatment (SP)

was carried out at +50°C (78). Alternatively, formaldehyde-fixed biopsies were subjected to high-pressure freezing, freeze-substitution and resin embedding as described for native cell samples (15), followed by standard incubations (60 min PA, 120 min TCH, 30 min SP at RT: (16)) – an approach, that yielded considerably intensified PAS-reaction product (Fig. 1F).

4.7. Electron microscopy and electron tomography

EM and tomography were described previously (15, 72).

Supplementary Material

Refer to Web version on PubMed Central for supplementary material.

Acknowledgments

We thank Jean Gruenberg (Genève) and the Developmental Studies Hybridoma Bank (created by the NICHD of the NIH and maintained at The University of Iowa, Department of Biology, Iowa City, IA 52242) for providing antibodies, as well as George Posthuma (Utrecht) for helpful discussion. This work was supported by the Austrian Science Fund (SFB021 to L.A.H.). The authors declare no competing financial interests.

References

1. Davidson GP, Cutz E, Hamilton JR, Gall DG. Familial enteropathy: a syndrome of protracted diarrhea from birth, failure to thrive, and hypoplastic villus atrophy. Gastroenterology. 1978; 75(5): 783–790. [PubMed: 100367]
2. Cutz E, Rhoads JM, Drumm B, Sherman PM, Durie PR, Forstner GG. Microvillus inclusion disease: an inherited defect of brush-border assembly and differentiation. N Engl J Med. 1989; 320(10):646–651. [PubMed: 2537465]
3. Phillips AD, Schmitz J. Familial microvillous atrophy: a clinicopathological survey of 23 cases. J Pediatr Gastroenterol Nutr. 1992; 14(4):380–396. [PubMed: 1355534]
4. Vogel GF, Hess MW, Pfaller K, Huber LA, Janecke AR, Muller T. Towards understanding microvillus inclusion disease. Mol Cell Pediatr. 2016; 3(1):3. [PubMed: 26830108]
5. Muller T, Hess MW, Schiefermeier N, Pfaller K, Ebner HL, Heinz-Erian P, Ponstingl H, Partsch J, Rollinghoff B, Kohler H, Berger T, Lenhartz H, Schlenck B, Houwen RJ, Taylor CJ, et al. MYO5B mutations cause microvillus inclusion disease and disrupt epithelial cell polarity. Nat Genet. 2008; 40(10):1163–1165. [PubMed: 18724368]
6. Wiegerinck CL, Janecke AR, Schneeberger K, Vogel GF, van Haaften-Visser DY, Escher JC, Adam R, Thoni CE, Pfaller K, Jordan AJ, Weis CA, Nijman IJ, Monroe GR, van Hasselt PM, Cutz E, et al. Loss of syntaxin 3 causes variant microvillus inclusion disease. Gastroenterology. 2014; 147(1):65–68. e10. [PubMed: 24726755]
7. Galvez-Santisteban M, Rodriguez-Fraticelli AE, Bryant DM, Vergarajauregui S, Yasuda T, Banon-Rodriguez I, Bernascone I, Datta A, Spivak N, Young K, Slim CL, Brakeman PR, Fukuda M, Mostov KE, Martin-Belmonte F. Synaptotagmin-like proteins control the formation of a single apical membrane domain in epithelial cells. Nat Cell Biol. 2012; 14(8):838–849. [PubMed: 22820376]
8. Trahair JF, Neutra MR, Gordon JI. Use of transgenic mice to study the routing of secretory proteins in intestinal epithelial cells: analysis of human growth hormone compartmentalization as a function of cell type and differentiation. J Cell Biol. 1989; 109(6 Pt 2):3231–3242. [PubMed: 2689454]
9. Troughton WD, Trier JS. Paneth and goblet cell renewal in mouse duodenal crypts. J Cell Biol. 1969; 41(1):251–268. [PubMed: 5775788]
10. Kataoka K. The fine structure of the proliferative cells of the mouse intestine as revealed by electron microscopic autoradiography with 3H-thymidine. Z Zellforsch Mikrosk Anat. 1970; 103(2):170–178. [PubMed: 5412826]

11. Moxey PC, Trier JS. Specialized cell types in the human fetal small intestine. Anat Rec. 1978; 191(3):269–285. [PubMed: 567022]
12. Phillips AD, Szafranski M, Man LY, Wall WJ. Periodic acid-Schiff staining abnormality in microvillous atrophy: photometric and ultrastructural studies. J Pediatr Gastroenterol Nutr. 2000; 30(1):34–42. [PubMed: 10630437]
13. Reinshagen K, Naim HY, Zimmer KP. Autophagocytosis of the apical membrane in microvillus inclusion disease. Gut. 2002; 51(4):514–521. [PubMed: 12235073]
14. Phillips AD, Brown A, Hicks S, Schuller S, Murch SH, Walker-Smith JA, Swallow DM. Acetylated sialic acid residues and blood group antigens localise within the epithelium in microvillous atrophy indicating internal accumulation of the glycocalyx. Gut. 2004; 53(12):1764–1771. [PubMed: 15542511]
15. Vogel GF, Klee KM, Janecke AR, Muller T, Hess MW, Huber LA. Cargo-selective apical exocytosis in epithelial cells is conducted by Myo5B, Slp4a, Vamp7, and Syntaxin 3. J Cell Biol. 2015; 211(3):587–604. [PubMed: 26553929]
16. Thiéry JP. Mise en évidence des polysaccharides sur coupes fines en microscopie électronique. J Microscopie (Paris). 1967; 6:987–1018.
17. Schneeberger K, Vogel GF, Teunissen H, van Ommen DD, Begthel H, El Bouazzaoui L, van Vugt AH, Beekman JM, Klumperman J, Muller T, Janecke A, Gerner P, Huber LA, Hess MW, Clevers H, et al. An inducible mouse model for microvillus inclusion disease reveals a role for myosin Vb in apical and basolateral trafficking. Proc Natl Acad Sci U S A. 2015; 112(40):12408–12413. [PubMed: 26392529]
18. Thoeni CE, Vogel GF, Tancevski I, Geley S, Lechner S, Pfaller K, Hess MW, Muller T, Janecke AR, Avitzur Y, Muise A, Cutz E, Huber LA. Microvillus inclusion disease: loss of Myosin vb disrupts intracellular traffic and cell polarity. Traffic. 2014; 15(1):22–42. [PubMed: 24138727]
19. Knowles BC, Roland JT, Krishnan M, Tyska MJ, Lapierre LA, Dickman PS, Goldenring JR, Shub MD. Myosin Vb uncoupling from RAB8A and RAB11A elicits microvillus inclusion disease. J Clin Invest. 2014; 124(7):2947–2962. [PubMed: 24892806]
20. Huber LA, Pimplikar S, Parton RG, Virta H, Zerial M, Simons K. Rab8, a small GTPase involved in vesicular traffic between the TGN and the basolateral plasma membrane. J Cell Biol. 1993; 123(1):35–45. [PubMed: 8408203]
21. Ang AL, Folsch H, Koivisto UM, Pypaert M, Mellman I. The Rab8 GTPase selectively regulates AP-1B-dependent basolateral transport in polarized Madin-Darby canine kidney cells. J Cell Biol. 2003; 163(2):339–350. [PubMed: 14581456]
22. He W, Ladinsky MS, Huey-Tubman KE, Jensen GJ, McIntosh JR, Bjorkman PJ. FcRn-mediated antibody transport across epithelial cells revealed by electron tomography. Nature. 2008; 455(7212):542–546. [PubMed: 18818657]
23. Puri C, Renna M, Bento CF, Moreau K, Rubinsztein DC. Diverse autophagosome membrane sources coalesce in recycling endosomes. Cell. 2013; 154(6):1285–1299. [PubMed: 24034251]
24. Lafont F, Verkade P, Galli T, Wimmer C, Louvard D, Simons K. Raft association of SNAP receptors acting in apical trafficking in Madin-Darby canine kidney cells. Proc Natl Acad Sci U S A. 1999; 96(7):3734–3738. [PubMed: 10097106]
25. Breuza L, Fransen J, Le Bivic A. Transport and function of syntaxin 3 in human epithelial intestinal cells. Am J Physiol Cell Physiol. 2000; 279(4):C1239–1248. [PubMed: 11003604]
26. Zhu D, Koo E, Kwan E, Kang Y, Park S, Xie H, Sugita S, Gaisano HY. Syntaxin-3 regulates newcomer insulin granule exocytosis and compound fusion in pancreatic beta cells. Diabetologia. 2013; 56(2):359–369. [PubMed: 23132338]
27. Ameen NA, Salas PJ. Microvillus inclusion disease: a genetic defect affecting apical membrane protein traffic in intestinal epithelium. Traffic. 2000; 1(1):76–83. [PubMed: 11208062]
28. Iancu TC, Mahajnah M, Manov I, Shaoul R. Microvillous inclusion disease: ultrastructural variability. Ultrastruct Pathol. 2007; 31(3):173–188. [PubMed: 17613997]
29. Ullrich O, Reinsch S, Urbe S, Zerial M, Parton RG. Rab11 regulates recycling through the pericentriolar recycling endosome. J Cell Biol. 1996; 135(4):913–924. [PubMed: 8922376]
30. Calhoun BC, Goldenring JR. Rab proteins in gastric parietal cells: evidence for the membrane recycling hypothesis. Yale J Biol Med. 1996; 69(1):1–8.

31. Barr FA. Review series: Rab GTPases and membrane identity: causal or inconsequential? J Cell Biol. 2013; 202(2):191–199. [PubMed: 23878272]
32. Urbe S, Huber LA, Zerial M, Tooze SA, Parton RG. Rab11, a small GTPase associated with both constitutive and regulated secretory pathways in PC12 cells. FEBS Lett. 1993; 334(2):175–182. [PubMed: 8224244]
33. Goldenring JR, Soroka CJ, Shen KR, Tang LH, Rodriguez W, Vaughan HD, Stoch SA, Modlin IM. Enrichment of rab11, a small GTP-binding protein, in gastric parietal cells. Am J Physiol. 1994; 267(2 Pt 1):G187–194. [PubMed: 8074219]
34. Thuenauer R, Hsu YC, Carvajal-Gonzalez JM, Deborde S, Chuang JZ, Romer W, Sonnleitner A, Rodriguez-Boulan E, Sung CH. Four-dimensional live imaging of apical biosynthetic trafficking reveals a post-Golgi sorting role of apical endosomal intermediates. Proc Natl Acad Sci U S A. 2014; 111(11):4127–4132. [PubMed: 24591614]
35. Weis GV, Knowles BC, Choi E, Goldstein AE, Williams JA, Manning EH, Roland JT, Lapierre LA, Goldenring JR. Loss of MYO5B in mice recapitulates Microvillus Inclusion Disease and reveals an apical trafficking pathway distinct to neonatal duodenum. Cell Mol Gastroenterol Hepatol. 2016; 2(2):131–157. [PubMed: 27019864]
36. Ruemmele FM, Muller T, Schiefermeier N, Ebner HL, Lechner S, Pfaller K, Thoni CE, Goulet O, Lacaille F, Schmitz J, Colomb V, Sauvat F, Revillon Y, Canioni D, Brousse N, et al. Loss-of-function of MYO5B is the main cause of microvillus inclusion disease: 15 novel mutations and a CaCo-2 RNAi cell model. Hum Mutat. 2010; 31(5):544–551. [PubMed: 20186687]
37. Hopkins CR, Gibson A, Shipman M, Strickland DK, Trowbridge IS. In migrating fibroblasts, recycling receptors are concentrated in narrow tubules in the pericentriolar area, and then routed to the plasma membrane of the leading lamella. J Cell Biol. 1994; 125(6):1265–1274. [PubMed: 7515888]
38. D'Souza S, Garcia-Cabado A, Yu F, Teter K, Lukacs G, Skorecki K, Moore HP, Orlowski J, Grinstein S. The epithelial sodium-hydrogen antiporter Na+/H+ exchanger 3 accumulates and is functional in recycling endosomes. J Biol Chem. 1998; 273(4):2035–2043. [PubMed: 9442041]
39. Ameen NA, Martensson B, Bourguinon L, Marino C, Isenberg J, McLaughlin GE. CFTR channel insertion to the apical surface in rat duodenal villus epithelial cells is upregulated by VIP in vivo. J Cell Sci. 1999; 112(Pt 6):887–894. [PubMed: 10036238]
40. Donowitz M, Li X. Regulatory binding partners and complexes of NHE3. Physiol Rev. 2007; 87(3):825–872. [PubMed: 17615390]
41. Ameen N, Silvis M, Bradbury NA. Endocytic trafficking of CFTR in health and disease. J Cyst Fibros. 2007; 6(1):1–14. [PubMed: 17098482]
42. Alexander RT, Grinstein S. Tethering, recycling and activation of the epithelial sodium-proton exchanger, NHE3. J Exp Biol. 2009; 212(Pt 11):1630–1637. [PubMed: 19448073]
43. Sato M, Grant BD, Harada A, Sato K. Rab11 is required for synchronous secretion of chondroitin proteoglycans after fertilization in Caenorhabditis elegans. J Cell Sci. 2008; 121(Pt 19):3177–3186. [PubMed: 18765566]
44. Wilson JD, Shelby SA, Holowka D, Baird B. Rab11 Regulates the Mast Cell Exocytic Response. Traffic. 2016; 17(9):1027–1041. [PubMed: 27288050]
45. van Ijzendoorn SC, Mostov KE, Hoekstra D. Role of rab proteins in epithelial membrane traffic. Int Rev Cytol. 2003; 232:59–88. [PubMed: 14711116]
46. Peranen J. Rab8 GTPase as a regulator of cell shape. Cytoskeleton (Hoboken). 2011; 68(10):527–539. [PubMed: 21850707]
47. Wandinger-Ness A, Zerial M. Rab proteins and the compartmentalization of the endosomal system. Cold Spring Harb Perspect Biol. 2014; 6(11):a022616. [PubMed: 25341920]
48. Henry L, Sheff DR. Rab8 regulates basolateral secretory, but not recycling, traffic at the recycling endosome. Mol Biol Cell. 2008; 19(5):2059–2068. [PubMed: 18287531]
49. Faust F, Gomez-Lazaro M, Borta H, Agricola B, Schrader M. Rab8 is involved in zymogen granule formation in pancreatic acinar AR42J cells. Traffic. 2008; 9(6):964–979. [PubMed: 18363906]
50. Sharma M, Giridharan SS, Rahajeng J, Naslavsky N, Caplan S. MICAL-L1 links EHD1 to tubular recycling endosomes and regulates receptor recycling. Mol Biol Cell. 2009; 20(24):5181–5194. [PubMed: 19864458]

51. Hampson A, O'Connor A, Smolenski A. Synaptotagmin-like protein 4 and Rab8 interact and increase dense granule release in platelets. J Thromb Haemost. 2013; 11(1):161–168.
52. Finetti F, Patrussi L, Galgano D, Cassioli C, Perinetti G, Pazour GJ, Baldari CT. The small GTPase Rab8 interacts with VAMP-3 to regulate the delivery of recycling T-cell receptors to the immune synapse. J Cell Sci. 2015; 128(14):2541–2552. [PubMed: 26034069]
53. Das S, Yu S, Sakamori R, Vedula P, Feng Q, Flores J, Hoffman A, Fu J, Stypulkowski E, Rodriguez A, Dobrowolski R, Harada A, Hsu W, Bonder EM, Verzi MP, et al. Rab8a vesicles regulate Wnt ligand delivery and Paneth cell maturation at the intestinal stem cell niche. Development. 2015; 142(12):2147–2162. [PubMed: 26015543]
54. Nakajo A, Yoshimura S, Togawa H, Kunii M, Iwano T, Izumi A, Noguchi Y, Watanabe A, Goto A, Sato T, Harada A. EHBP1L1 coordinates Rab8 and Bin1 to regulate apical-directed transport in polarized epithelial cells. J Cell Biol. 2016; 212(3):297–306. [PubMed: 26833786]
55. Stenmark H. Rab GTPases as coordinators of vesicle traffic. Nat Rev Mol Cell Biol. 2009; 10(8): 513–525. [PubMed: 19603039]
56. Roland JT, Kenworthy AK, Peranen J, Caplan S, Goldenring JR. Myosin Vb interacts with Rab8a on a tubular network containing EHD1 and EHD3. Mol Biol Cell. 2007; 18(8):2828–2837. [PubMed: 17507647]
57. Rowe RK, Suszko JW, Pekosz A. Roles for the recycling endosome, Rab8, and Rab11 in hantavirus release from epithelial cells. Virology. 2008; 382(2):239–249. [PubMed: 18951604]
58. Westlake CJ, Baye LM, Nachury MV, Wright KJ, Ervin KE, Phu L, Chalouni C, Beck JS, Kirkpatrick DS, Slusarski DC, Sheffield VC, Scheller RH, Jackson PK. Primary cilia membrane assembly is initiated by Rab11 and transport protein particle II (TRAPPII) complex-dependent trafficking of Rabin8 to the centrosome. Proc Natl Acad Sci U S A. 2011; 108(7):2759–2764. [PubMed: 21273506]
59. Bryant DM, Datta A, Rodriguez-Fraticelli AE, Peranen J, Martin-Belmonte F, Mostov KE. A molecular network for de novo generation of the apical surface and lumen. Nat Cell Biol. 2010; 12(11):1035–1045. [PubMed: 20890297]
60. Roman-Fernandez A, Bryant DM. Complex Polarity: Building Multicellular Tissues Through Apical Membrane Traffic. Traffic. 2016
61. Zhen Y, Stenmark H. Cellular functions of Rab GTPases at a glance. J Cell Sci. 2015; 128(17): 3171–3176. [PubMed: 26272922]
62. Baetz NW, Goldenring JR. Rab11-family interacting proteins define spatially and temporally distinct regions within the dynamic Rab11a-dependent recycling system. Mol Biol Cell. 2013; 24(5):643–658. [PubMed: 23283983]
63. Baetz NW, Goldenring JR. Distinct patterns of phosphatidylserine localization within the Rab11a-containing recycling system. Cell Logist. 2014; 4:e28680. [PubMed: 25210648]
64. Phillips A, Fransen J, Hauri HP, Sterchi E. The constitutive exocytotic pathway in microvillous atrophy. J Pediatr Gastroenterol Nutr. 1993; 17(3):239–246. [PubMed: 8271121]
65. Janecke AR, Heinz-Erian P, Yin J, Petersen BS, Franke A, Lechner S, Fuchs I, Melancon S, Uhlig HH, Travis S, Marinier E, Perisic V, Ristic N, Gerner P, Booth IW, et al. Reduced sodium/proton exchanger NHE3 activity causes congenital sodium diarrhea. Hum Mol Genet. 2015; 24(23):6614–6623. [PubMed: 26358773]
66. Janecke AR, Heinz-Erian P, Muller T. Congenital Sodium Diarrhea: A Form of Intractable Diarrhea, With a Link to Inflammatory Bowel Disease. J Pediatr Gastroenterol Nutr. 2016; 63(2): 170–176. [PubMed: 26835907]
67. Muller T, Rasool I, Heinz-Erian P, Mildenberger E, Hulstrunk C, Muller A, Michaud L, Koot BG, Ballauff A, Vodopiutz J, Rosipal S, Petersen BS, Franke A, Fuchs I, Witt H, et al. Congenital secretory diarrhoea caused by activating germline mutations in GUCY2C. Gut. 2016; 65(8):1306–1313. [PubMed: 25994218]
68. Kravtsov DV, Ahsan MK, Kumari V, van Ijzendoorn SC, Reyes-Mugica M, Kumar A, Gujral T, Dudeja PK, Ameen NA. Identification of intestinal ion transport defects in microvillus inclusion disease. Am J Physiol Gastrointest Liver Physiol. 2016; 311(1):G142–155. [PubMed: 27229121]

69. Lapierre LA, Ducharme NA, Drake KR, Goldenring JR, Kenworthy AK. Coordinated regulation of caveolin-1 and Rab11a in apical recycling compartments of polarized epithelial cells. Exp Cell Res. 2012; 318(2):103–113. [PubMed: 22036648]

70. Goldenring JR, Smith J, Vaughan HD, Cameron P, Hawkins W, Navarre J. Rab11 is an apically located small GTP-binding protein in epithelial tissues. Am J Physiol. 1996; 270(3 Pt 1):G515–525. [PubMed: 8638719]

71. Lapierre LA, Avant KM, Caldwell CM, Oztan A, Apodaca G, Knowles BC, Roland JT, Ducharme NA, Goldenring JR. Phosphorylation of Rab11-FIP2 regulates polarity in MDCK cells. Mol Biol Cell. 2012; 23(12):2302–2318. [PubMed: 22553350]

72. Vogel GF, Ebner HL, de Araujo ME, Schmiedinger T, Eiter O, Pircher H, Gutleben K, Witting B, Teis D, Huber LA, Hess MW. Ultrastructural Morphometry Points to a New Role for LAMTOR2 in Regulating the Endo/Lysosomal System. Traffic. 2015; 16(6):617–634. [PubMed: 25677580]

73. Berod A, Hartman BK, Pujol JF. Importance of fixation in immunohistochemistry: use of formaldehyde solutions at variable pH for the localization of tyrosine hydroxylase. J Histochem Cytochem. 1981; 29(7):844–850. [PubMed: 6167611]

74. Tokuyasu KT. A technique for ultracryotomy of cell suspensions and tissues. J Cell Biol. 1973; 57(2):551–565. [PubMed: 4121290]

75. Liou W, Geuze HJ, Slot JW. Improving structural integrity of cryosections for immunogold labeling. Histochem Cell Biol. 1996; 106(1):41–58. [PubMed: 8858366]

76. Ripper D, Schwarz H, Stierhof YD. Cryo-section immunolabelling of difficult to preserve specimens: advantages of cryofixation, freeze-substitution and rehydration. Biol Cell. 2008; 100(2):109–123. [PubMed: 17903123]

77. Wickstrom SA, Lange A, Hess MW, Polleux J, Spatz JP, Kruger M, Pfaller K, Lambacher A, Bloch W, Mann M, Huber LA, Fassler R. Integrin-linked kinase controls microtubule dynamics required for plasma membrane targeting of caveolae. Dev Cell. 2010; 19(4):574–588. [PubMed: 20951348]

78. Neiss WF. Enhancement of the periodic acid--Schiff (PAS) and periodic acid--thiocarbohydrazide--silver proteinate (PA-TCH-SP) reaction in LR white sections. Histochemistry. 1988; 88(3–6):603–612. [PubMed: 2835340]

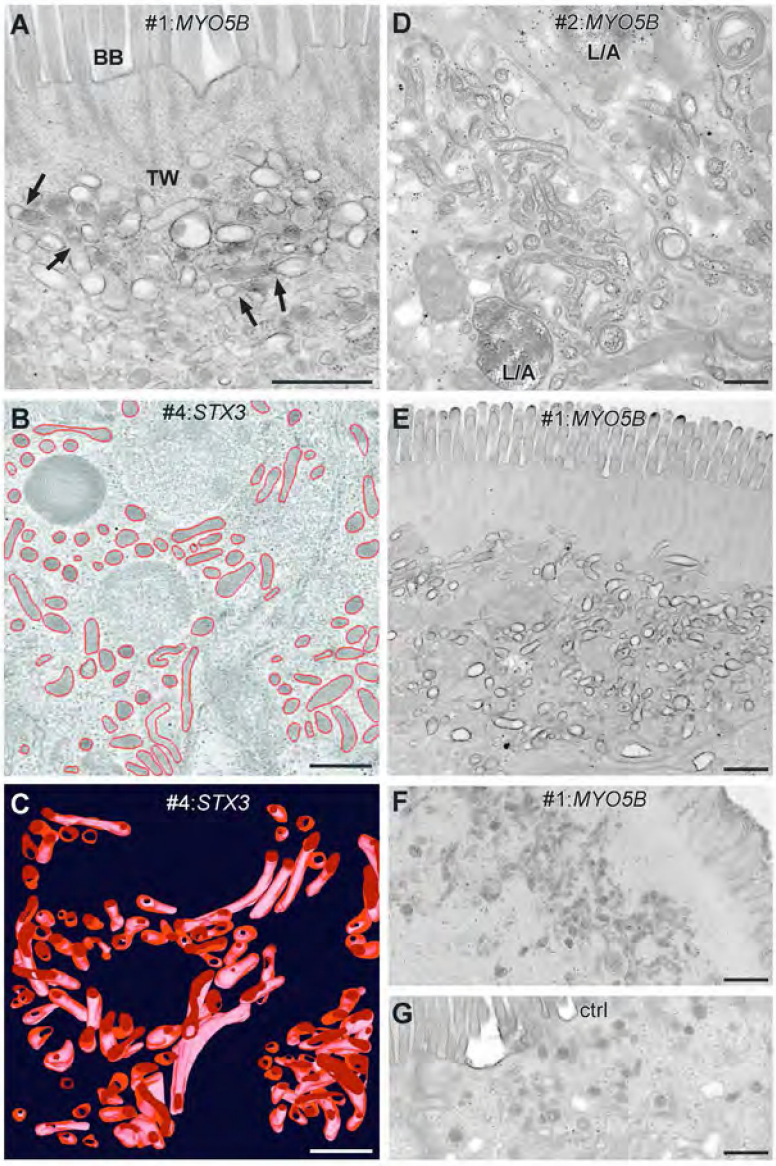

Figure 1. Ultrastructure, 3D-architecture and PAS-cytochemistry of subapical vesicles/tubules (representing the historically termed "secretory granules") as seen in plastic sections from small intestinal biopsies of MVID and control patients (scale bars = 500nm)

A. Vesicular and tubular endomembrane compartments with electron-dense or -translucent contents below the brush border and terminal web (BB, TW) of villus enterocytes from a duodenum biopsy of MVID patient #1; transitions between dense and lucent compartments marked by arrows; standard uranyl acetate/lead section staining;

B. 2D slice from an electron tomographic reconstruction with contour lining (red) of dense compartments in a villus cell of patient #4 (taken from Movie S1); jejunum;

C. 3D model of the dense compartments outlined in Figure 1B; patient #4;

D. Cytochemical detection of darkly stained PAS-reactive material within tubular compartments and (autophago)lysosomes (L/A) in patient #2; duodenum, villus cell;

E. Villus enterocyte from duodenum of patient #1 with only moderate PAS-reactivity of dense and lucent compartments after standard sample processing;
F. Same biopsy from patient #1 as in Figure 1E, but subjected to freeze-substitution instead of standard processing: distinct PAS-reactivity of subapical compartments is recognizable;
G. Control section from a patient with non-MVID related intestinal disease showing scattered PAS-positive, putative “secretory granules” in the periphery of a crypt enterocyte.

Figure 2. Graphic representation (generalized) of ultrastructural features characterizing the enterocytes from MVID patients with mutated *MYO5B* or *STX3*

Villus enterocytes of MVID patients with *MYO5B* mutations are generally characterized by (i) subapical vesiculo-tubular endomembrane accumulations, historically termed “secretory granules” (shown in orange), (ii) brush-border microvilli (shown in green) that are locally greatly reduced in size and frequency, (iii) microvillus inclusions (and/or sporadic basolateral microvilli) and (iv) numerous, large (autophago)lysosomes (shown in brown). Villus enterocytes of patients with mutated *STX3* show regularly (i) abundant subapical vesicles and tubules, (ii) facultative brush-border disintegration, (iii) ectopic microvilli, predominantly forming basolateral bundles (rather than lining cytoplasmic microvillus inclusions), (iv) (autophago)lysosomes. Undifferentiated crypt enterocytes of patients with mutated *MYO5B* or *STX3* display (i) more or less prominent subapical clusters of vesicles and tubules, (ii) varying configurations of apical microvilli that appear either reduced in size and number (*STX3* mutations) or normal (*MYOB* mutations). Healthy villus and crypt enterocytes are shown for comparison.

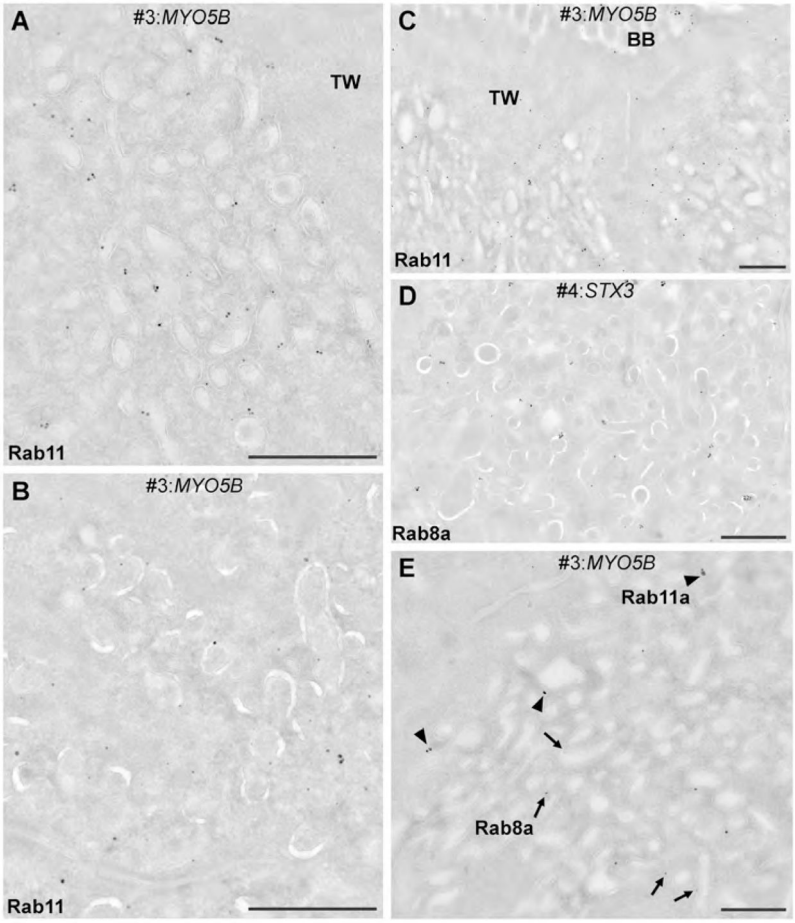

Figure 3. Rab11 and Rab8 immunogold labelling of thawed ultra-thin cryo-sections from duodenum biopsies of MVID-patients (scale bars = 500nm)

A. Rab11 label of subapical vesicular and tubular endomembrane compartments with electron-lucent contents; villus cell of patient #3;

B. Rab11 label at dense compartments; crypt cell of patient #3;

C. Overview of Rab11 distribution in the (sub)apical region of villus enterocytes from patient #3;

D. Rab8a label at dense compartments in a crypt cell of patient #4;

E. Rab11a (arrow-heads) and Rab8a (arrows) label at membranes of subapical vesicles/tubules in a villus cell of patient #3.

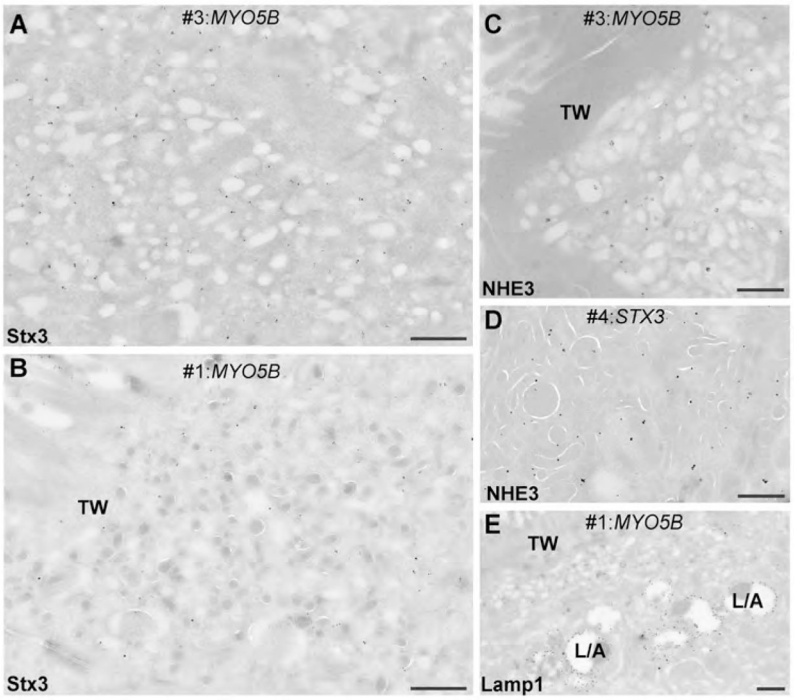

Figure 4. Immunogold labelling of Stx3, NHE3 and Lamp1 in enterocytes of the small intestine from MVID-patients (cryo-sections; scale bars = 500nm)

A. Stx3 label throughout the subapical vesicle/tubule clusters in a villus cell of patient #3;

B. Stx3 label in the periphery of a villus cell from patient #1;

C. NHE3 label in a villus cell from patient #3;

D. NHE3 labelling of membranes, but locally also contents of the dense endomembrane compartments in a crypt cell from patient #4;

E. Lamp1 labelling of (autophago)lysosomes (L/A), but not subapical vesicles/tubules in a villus cell from patient #1.

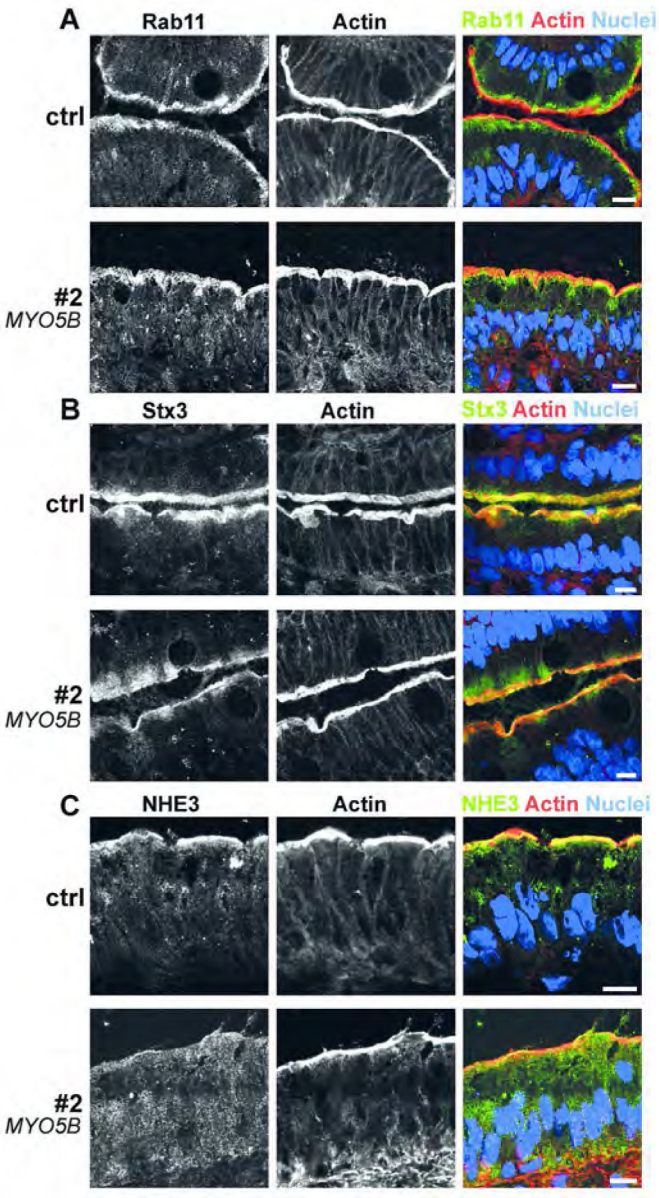

Figure 5. (Immuno-)fluorescence microscopy of duodenum biopsies from patient #2 and control (cryostat sections)

Rab11 (Figure 5A), Stx3 (Figure 5B) and NHE3 (Figure 5C) show diffuse staining throughout the subapical cytoplasm of the patient's enterocytes, in addition to, or instead of their normal localization (Rab11, Stx3 or NHE3, respectively); scale bar = 10μm.

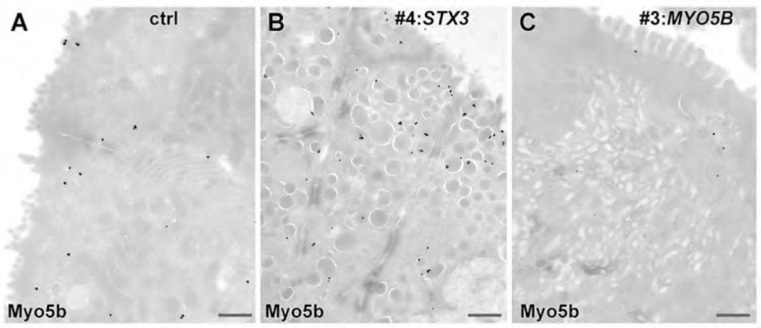

Figure 6. Immunogold labelling of Myo5b in enterocytes from MVID- and control patients (cryo-sections; scale bars = 500nm)

A. Diffuse Myo5b label throughout the apical cytoplasm in a villus cell of a control patient.

B. Myo5b label predominantly associated with vesicular endomembranes in the (sub)apical cytoplasm of a colon crypt cell from patient #4 with mutated *STX3*.

C. Virtual no Myo5b label in a villus cell from patient #3 with mutated *MYO5B*.

Table 1

Synoptic view on the here presented MVID patients and CaCo2 cell models with mutated *MYO5B* or *STX3* demonstrating the variability of ultrastructural alterations of small intestine enterocytes.

	patient/gene/mutation				**CaCo2 cell lines *)**	
	#1: *MYO5B* c.244G>A (p.Glu82Lys)	**#2: *MYO5B* c.414C>A (p.His138Gln)**	**#3: *MYO5* c.1323–2A>G [Refs. (17, 4)]**	**#4: *STX3* c.372_373dup (p.Arg125Leufs*7) [Ref. (6)]**	**Myo5B KI 1125 G>A [Ref. (15)]**	**mCitrine-STX3: AA1-125; mCitrine-STX3: AA1-247 [Ref. (6)]**
Lucent Vesicles/Tubules: Villus	++	+++	+++	+++	+++	+++
Lucent Vesicles/Tubules: Crypt	+	–	++	–		
Dense Vesicles/Tubules: Villus	++	+ (+)	+	++	+	+
Dense Vesicles/Tubules: Crypt	+	+	+++	+++		
Denuded enterocytes: Villus	+	+	+++	++	+++	+++
Denuded enterocytes: Crypt	–	–	–	+++		
Microvillous Inclusions	+	+	+++	+	++	+
Basolateral Microvilli	–	+	++	++	+	+++

+++ … abundant

++… regular

+… sporadic

–… not observed

*)… % Distinction villus *VS.* crypt cells not applicable

Comments:

- **i.** Obvious correlations between clinical symptoms, mutations and ultrastructural features were not evident in these cases.
- **ii.** Gross morphology of small intestinal biopsies from patient #1 and #2 did not show villus atrophy.

Table 2

Immunoelectron and PAS-cytochemical characteristics of subcellular compartments in enterocytes from MVID patients with mutated *MYO5B* or *STX3* and control patients

	Rab11/Rab8			Stx3			NHE3			LAMP1			PAS		
	MYO5B	***STX3***	**Ctrl.**	***MYO5B***	***STX3***	**Ctrl.**	***MYO5B***	***STX3***	**Ctrl.**	***MYO5B***	***STX3***	**Ctrl.**	***MYO5B***	***STX3***	**Ctrl.**
Subapical Vesicles/Tubules in MVID	+	+		+	–		+	+		s	s		+	+	
canonical “Secretory Granules” (crypt)			+			–/?			s/?			–			+
canonical Recycling Endosomes			+			s			s			–			+
Late Endosomes, (Autophago-) Lysosomes	–	–	–	–	–	–	–	–	–	+	+	+	+	+	+
Trans Golgi Network	+	+	+	+	–	+	–	–	–	+	+	+	+	+	+
Endoplasmic Reticulum	–	–	–	–	–	–	+	+	+	–	–	–	–	–	–
undefined endomembranes a/o cytoplasm	+	+	+	+	–	s	+	+	+	–	–	–	–	–	–
Plasma Membrane	+	+	+	+	–	+	+	+	+	–	–	–	+	+	+

+… distinct label

–… no label

s… sporadic label

empty fields: specified organelles not discernible (or missing)